

Conformational Regulation of Multivalent Terpyridine Ligands for Self-Assembly of Heteroleptic Metallo-Supramolecules

Shi-Cheng Wang, Kai-Yu Cheng, Jun-Hao Fu, Yuan-Chung Cheng, and Yi-Tsu Chan*



Cite This: *J. Am. Chem. Soc.* 2020, 142, 16661–16667



Read Online

ACCESS |



Metrics & More

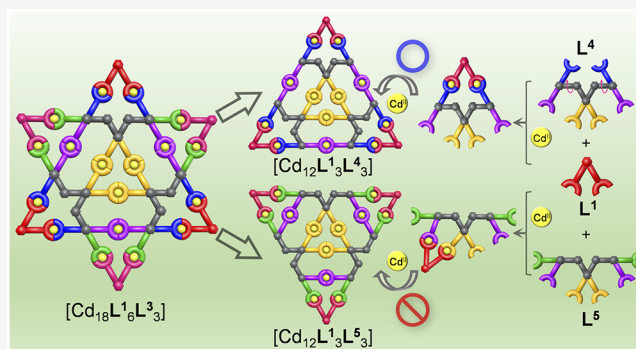


Article Recommendations



Supporting Information

ABSTRACT: A two-ligand system composed of the predesigned multivalent and complementary terpyridine-based ligands was exploited to construct heteroleptic metallo-supramolecules and to investigate the self-assembly mechanism. Molecular stellation of the trimeric hexagon $[\text{Cd}_6\text{L}^2_3]$ gave rise to the exclusive self-assembly of the star hexagon $[\text{Cd}_{18}\text{L}^1_6\text{L}^3_3]$ through complementary ligand pairing between the ditopic and octatopic tectons. To understand how the intermolecular heteroleptic complexation influenced the self-assembly pathway, the star hexagon was truncated into two triangular fragments: $[\text{Cd}_{12}\text{L}^1_3\text{L}^4_3]$ and $[\text{Cd}_{12}\text{L}^1_3\text{L}^5_3]$. In the self-assembly of $[\text{Cd}_{12}\text{L}^1_3\text{L}^4_3]$, the conformational movements of hexatopic ligand L^4 could be regulated by L^1 to promote the subsequent coordination event, which was the key step to the successful multicomponent self-assembly. In contrast, the formation of $[\text{Cd}_{12}\text{L}^1_3\text{L}^5_3]$ was hampered by the geometrically mismatched intermediates.



INTRODUCTION

Cooperative self-assembly prevails ubiquitously in construction and modulation of functional biomacromolecules in nature.¹ The cooperativity typically involves conformational regulation of receptors² or configurational preorganization of two or more building blocks³ to either increase or decrease binding affinity in subsequent binding events. The bio-inspired molecular design with cooperativity has been demonstrated in creation of artificial systems for applications in molecular recognition,⁴ catalysis,⁵ ion sensing,⁶ and so on. Besides, such a strategy could be applied to synthesis of sophisticated supramolecules in a well-controlled manner.⁷ However, it still remains a challenge to rationally design molecular building blocks for manipulation of inter- and intramolecular cooperative interactions.

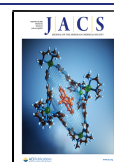
Well-defined metal–ligand coordination geometry provides directional bonding to assemble molecular subcomponents in a preprogrammed way, which is a promising approach for construction of metallo-supramolecules.⁸ Aiming to further enhance geometrical diversity and complexity of assemblies, comprehension of self-assembly mechanisms⁹ and development of high-fidelity molecular recognition tools are essential for preventing the formation of undesired products in a multicomponent system. Hence, several self-selective coordination strategies have been developed for mono-,¹⁰ bi-,¹¹ and tridentate¹² ligands to fulfill the requirements. Among them, a variety of multivalent 2,2':6',2''-terpyridine (tpy)-based ligands can be obtained by palladium-catalyzed cross-coupling reactions¹³ and serve as subcomponents for self-assembly of

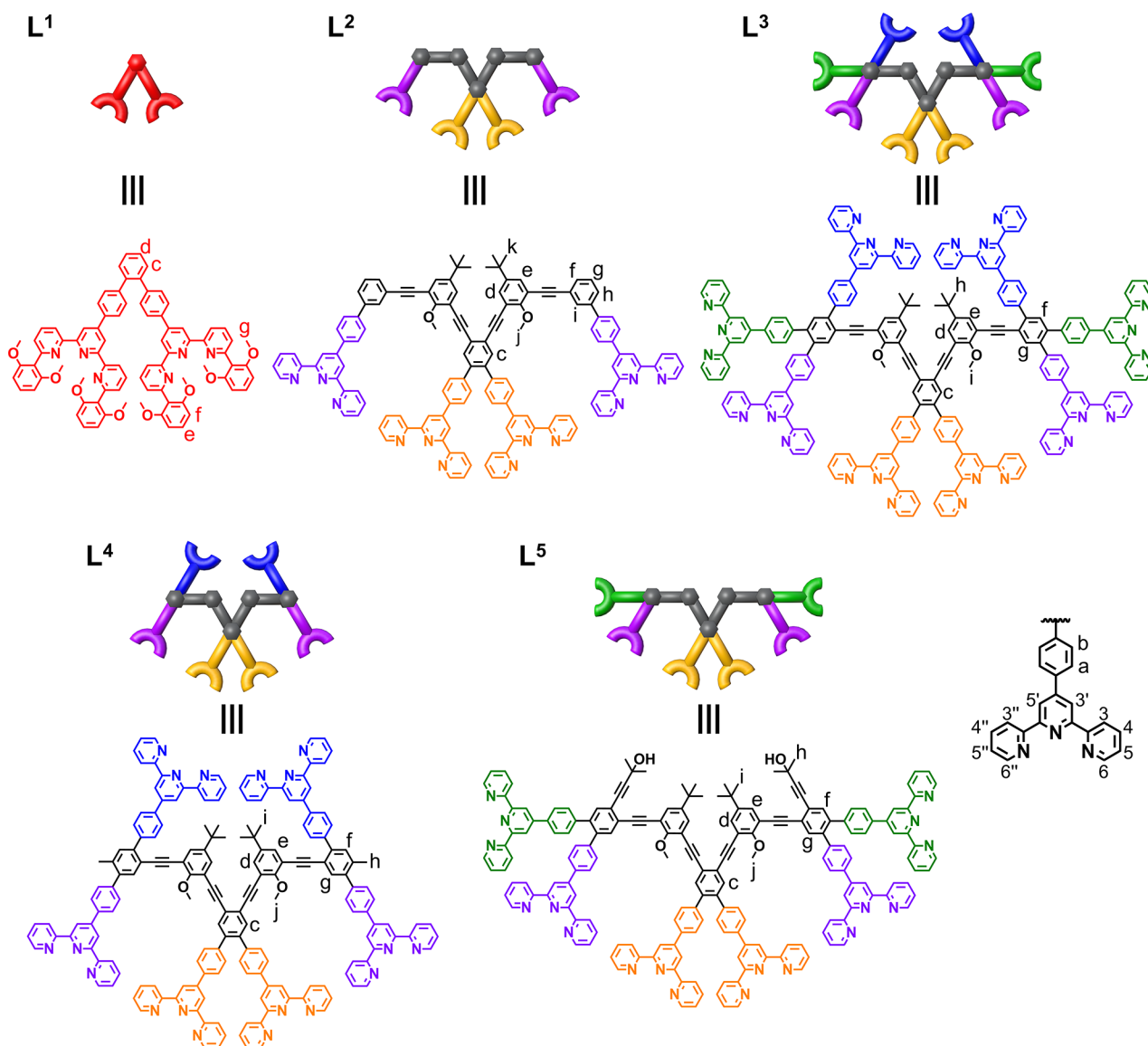
giant metallo-supramolecules.¹⁴ In the supramolecular chemistry of metal–tpy complexes, a stepwise approach is commonly used to prepare predesigned metalloligands to eliminate mismatched assemblies during self-assembly.^{8e,15} Nevertheless, toward elevating the degree of molecular self-sorting,¹⁶ we have demonstrated that an equimolar mixture of 6,6''-di(2,6-dimethoxyphenyl)tpy and unsubstituted tpy ligands can afford a sole heteroleptic complex upon addition of Cd^{II} ions under ambient conditions.^{12c} The complementary ligand pair offers facile access to preparation of discrete metallomacrocycles as well as metallocages via multicomponent self-assembly.^{12e,17}

To elucidate the importance of conformational regulation of multivalent ligands by intermolecular heteroleptic complexation, which resembles cooperative self-assembly in nature, herein we design and synthesize a suite of multivalent ligands L^2 – L^5 and investigate the interplay in assembling with the complementary ligand L^1 . The star hexagon $[\text{Cd}_{18}\text{L}^1_6\text{L}^3_3]$ consisting of the hexagonal core $[\text{Cd}_6\text{L}^2_3]$ is constructed in excellent yield via one-pot heteroleptic complexation. The self-assembly behavior of triangular fragments $[\text{Cd}_{12}\text{L}^1_3\text{L}^4_3]$ and

Received: June 19, 2020

Published: September 3, 2020



Scheme 1. Chemical Structures and Cartoon Representations of Ligands L¹, L², L³, L⁴, and L⁵

[Cd₁₂L₃L₅] derived from [Cd₁₈L₆L₃] is examined by titration experiments. The result indicates that the selective intermolecular complexation between L¹ and L⁴ leads to an appropriate conformation of tetratopic intermediate [Cd₂L¹L⁴], which allows for the formation of the desired product.

RESULTS AND DISCUSSION

The 6,6''-substituted bis-tpy ligand L¹ was prepared following the reported protocol.^{12c} Multivalent ligands L², L³, L⁴, and L⁵ (Scheme 1) were synthesized through a series of Pd-catalyzed Sonogashira and Suzuki–Miyaura coupling reactions (Schemes S1–S4), and the structural characterization was carefully done by NMR spectroscopy (Figures S1–S25) and high-resolution MALDI-TOF mass spectrometry (Figures S30–S33). The self-assembly experiment started with the tetratopic ligand L², which was reacted with 2 equiv of Cd(NO₃)₂ in CHCl₃/MeOH (1/1, v/v) at 25 °C for 30 min. The reaction mixture was counterion-exchanged with excess NH₄PF₄ and then stirred at 25 °C for an additional 30 min (Figure 1a). After complexation, the ¹H NMR spectrum of the resultant complex

remained sharp and well split. In the aromatic region, in contrast to the downfield shifts of most of the signals, two doublets from 6,6''-tpy protons exhibited significant upfield shifts, indicating the formation of the octahedral coordination geometry of <tpy-Cd^{II}-tpy> connectivity.¹⁸ Two sets of tpy signals with an integration ratio of 1:1 could be identified by using COSY and ROESY NMR techniques (Figures S37 and S38). Particularly, in the ROESY spectrum, the singlet from Hⁱ showed the correlation signal to the purple-labeled phenylene protons H^b so that two types of the bistpy complexes in the assembly could be unambiguously assigned. The methoxy groups (H^j) and *tert*-butyl groups (H^k) still revealed sharp singlets after complexation (Figure S35), supporting the formation of a highly symmetric structure. In addition, the two ¹¹³Cd NMR singlets at δ 268.80 and 267.77 ppm clearly indicated that the self-assembly has two kinds of Cd^{II} centers (Figure S55). All the related peaks in the DOSY spectrum possessing the same diffusion coefficient ($D = 3.29 \times 10^{-10} \text{ m}^2 \text{ s}^{-1}$) proved the formation of a single self-assembled structure in solution (Figure S51).

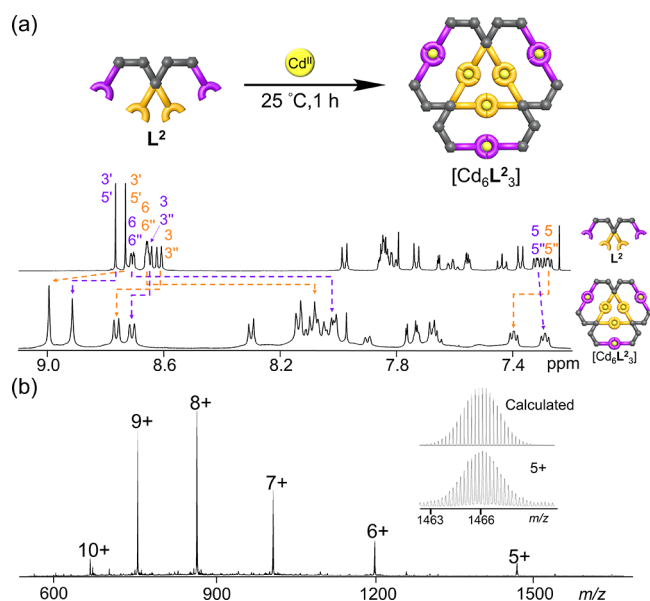


Figure 1. (a) Self-assembly of trimeric hexagon [Cd₆L₂³] and ¹H NMR spectra of L² and [Cd₆L₂³]. (b) ESI-MS spectrum of [Cd₆L₂³] and isotopic pattern of [M - 5PF₆]³⁺.

High-resolution electrospray ionization mass spectrometry (HR-ESI-MS) was used to verify the chemical composition of the complex. The ESI spectrum showed one series of peaks in agreement with the ions of trimeric hexagon [Cd₆L₂³] at charge states from 5+ to 10+ (Figure 1b). In addition, electrospray ionization coupled with traveling wave ion-mobility mass spectrometry (ESI-TWIM-MS) was utilized to obtain additional structural information.¹⁹ The ESI-TWIM-MS plot of [Cd₆L₂³] demonstrated a narrow drift time distribution for each charge state, indicating the absence of isomeric structures (Figure S61).²⁰ The consistent correlation between the experimental and theoretical collision cross sections (CCSs) supported the presence of the proposed structure (Figure S63 and Table S2).

In geometrical stellation,²¹ a star hexagon can be produced by extending the edges of a hexagon until they intersect to form the new closed boundaries. On the basis of the successful self-assembly of [Cd₆L₂³], we anticipated that a more complicated star-shaped metallo-supramolecule would be achieved through the complementary ligand pairing^{12c-e} between ligands L¹ and L³. As compared with L², the octatopic ligand L³ has four additional coordination units to pair with L¹ to form the external triangles. The complexation reaction of L¹, L³, and Cd^{II} ions in a precise molar ratio of 2:1:6 was conducted to examine the multicomponent self-assembly process. As expected, the ¹H NMR spectrum of the resultant complex (Figure 2a) displayed two kinds of chemical environments for ligand L¹. Particularly, the peaks for the 3',5'-tpp protons and the 2,6-dimethoxyphenyl substituents (H^e and H^f) were split into two signals with an integration ratio of 1:1, suggesting the formation of two distinct heteroleptic complexes. The proper assignments for six sets of tpp protons, including two homoleptic and two heteroleptic complexes, were verified by COSY and ROESY experiments (Figures S39–S42). It is noteworthy that two triplets from the blue and green 5,5''-tpp protons of L³ were assigned according to the ROESY spatial correlation with methoxy groups H^g of L¹, and the two heteroleptic connections were distinguished by

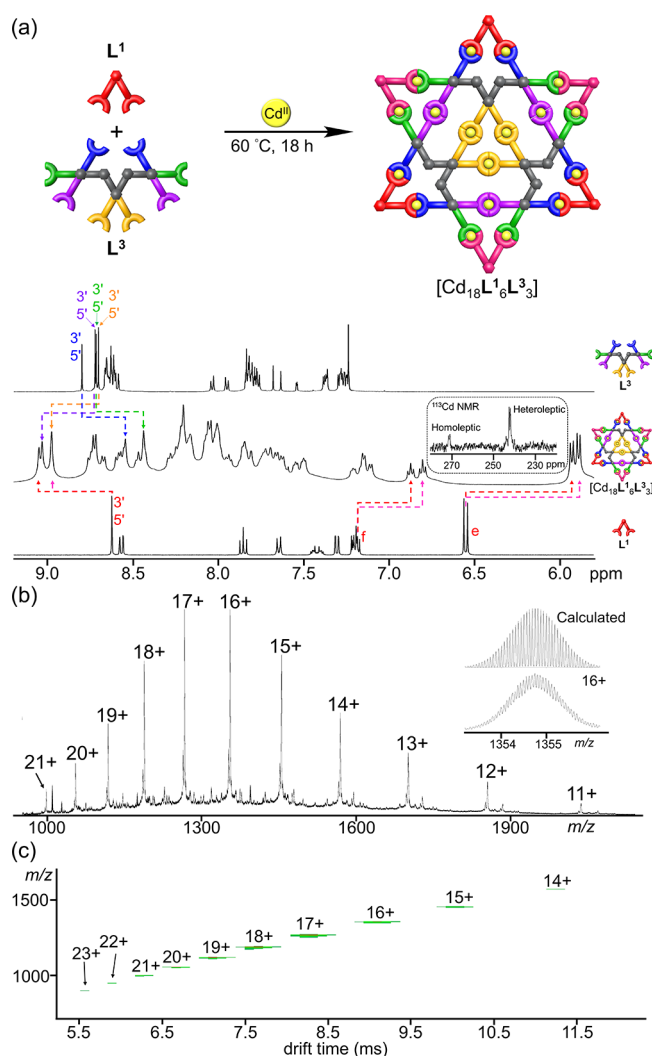


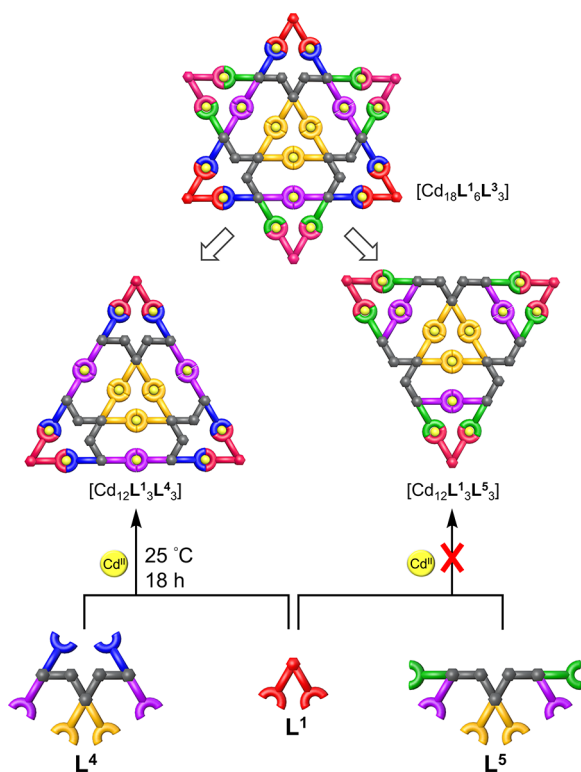
Figure 2. (a) Self-assembly of star hexagon [Cd₁₈L¹₆L³₃] and ¹H NMR spectra of L³, [Cd₁₈L¹₆L³₃], and L¹. The inset is the ¹¹³Cd NMR spectrum of [Cd₁₈L¹₆L³₃]. (b) ESI-MS spectrum and (c) ESI-TWIM-MS plot of [Cd₁₈L¹₆L³₃].

the correlation with *tert*-butyl groups H^h of L³ (Figure S42). Relative to the uncomplexed L³, the blue and green 3',5'-tpp protons exhibited significant upfield shifts due to the shielding effect deduced from the 2,6-dimethoxyphenyl substituents;^{12c} on the other hand, the orange and purple 3',5'-tpp protons showed downfield shifts because of coordination to the electron-deficient Cd^{II} ions (Figure 2a). Consistently, the ¹¹³Cd NMR analysis (Figure 2a and Figure S56) revealed two signals at δ 271.83 and 271.21 ppm and two peaks at δ 242.66 and 242.06 ppm with a 1:2 integration ratio, corresponding to the homoleptic and heteroleptic connections, respectively. The DOSY NMR spectrum indicated the existence of a sole species with $D = 1.36 \times 10^{-10} \text{ m}^2 \text{ s}^{-1}$ in CD₃CN (Figure S52). Eventually, the formulation of [Cd₁₈L¹₆L³₃] was confirmed by 11 ESI-MS peaks derived from 11+ to 21+ ions (Figure 2b). In the ESI-TWIM-MS plot (Figure 2c), a single stair pattern with narrow drift time distributions implied that a discrete and rigid molecular star was assembled. The experimental average CCS also agreed well with the theoretical average CCSs generated from 300 simulated conformations (Figure S64 and Table S3).

To shed light on the self-assembly mechanism of [Cd₁₈L¹₆L³₃], the star-shaped complex was chopped into two

triangular fragments (Scheme 2) and their self-assembly processes were examined. Ligands L^4 and L^5 were synthesized

Scheme 2. Self-Assembly of Triangular Fragments $[Cd_{12}L^1_3L^4_3]$ and $[Cd_{12}L^1_3L^5_3]$



by attaching two 4-terpyridylphenyl units at the *para* and *ortho* positions with respect to the purple-labeled 4-terpyridylphenyl substituents, respectively (Scheme 1). For construction of $[Cd_{12}L^1_3L^4_3]$, the hexatopic ligand L^4 was assembled with L^1 in the presence of Cd^{II} ions. It was found that the desired triangle was produced in excellent yield under mild conditions.

The 1H NMR characterization (Figure 3a) of $[Cd_{12}L^1_3L^4_3]$ exhibited three significant upfield shifts for the 2,6-dimethoxyphenyl protons (H^e and H^f) of L^1 and the blue-labeled 3',5'-tpy portions of L^4 as compared to the uncoordinated L^1 and L^4 , which were similar to the observation in $[Cd_{18}L^1_6L^3_3]$ that indicated the formation of the heteroleptic connectivity. The exclusive formation of the target complex was confirmed by five distinct 1H NMR singlets at δ 9.04 ppm (purple 3',5'-tpy H_s of L^4), 9.02 ppm (3',5'-tpy H_s of L^1), 8.93 ppm (orange 3',5'-tpy H_s of L^4), 8.47 ppm (blue 3',5'-tpy H_s of L^4), and 4.32 ppm (OCH_3 of L^4) as well as three ^{113}Cd NMR peaks at δ 270.91, 269.98, and 241.35 ppm derived from two homoleptic and one heteroleptic Cd^{II} nuclei (Figure 3a and Figure S57). The complete assignments were established by COSY and ROESY NMR (Figures S43–S46). The DOSY NMR spectrum (Figure S53) showed that all the relevant signals have the same diffusion coefficient ($D = 2.89 \times 10^{-10} m^2 s^{-1}$). The assembled composition of $[Cd_{12}L^1_3L^4_3]$ was unequivocally determined by the intense ESI-MS peaks generated from the 8+ to 16+ ions (Figure 3b), and its experimental average CCS of 1965.6 ± 7.6 obtained from the TWIM-MS analysis (Figure S62) was consistent with the modeled ones (Figure S65 and Table S4).

The complexation reaction of L^1 (1 equiv), L^5 (1 equiv), and Cd^{II} ions (4 equiv) was conducted at 60 °C to construct

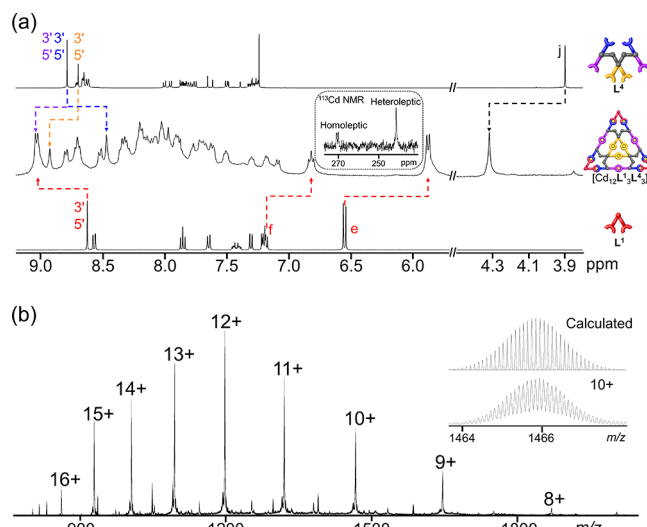
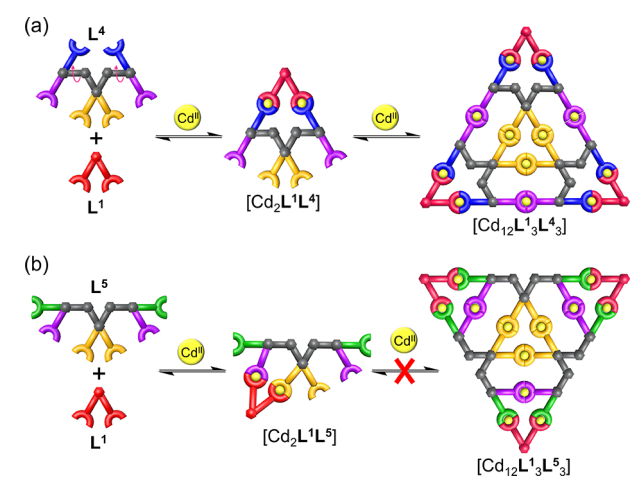


Figure 3. (a) 1H NMR spectra of L^4 , $[Cd_{12}L^1_3L^4_3]$, and L^1 . The inset is the ^{113}Cd NMR spectrum of $[Cd_{12}L^1_3L^4_3]$. (c) ESI-MS spectrum of $[Cd_{12}L^1_3L^4_3]$ and isotope pattern of $[M - 10PF_6]^{10+}$.

$[Cd_{12}L^1_3L^5_3]$ (Scheme 2). However, the resultant complex exhibited relatively poor solubility in common organic solvents, such as MeOH, MeCN, and MeNO₂. The 1H NMR spectrum (Figure S47) showed broad signals, which could not be properly identified and displayed multiple diffusion distributions ($D = (4.47–4.90) \times 10^{-10} m^2 s^{-1}$) in the DOSY experiment (Figure S54). The corresponding hydrodynamic radii were much smaller than those of $[Cd_6L^2_3]$, $[Cd_{12}L^1_3L^4_3]$, and $[Cd_{18}L^1_6L^3_3]$ (Table S1). The ESI-MS spectrum (Figure S58) revealed that at least two species $[Cd_{12}L^1_3L^5_3]$ and $[Cd_{10}L^1_4L^5_2]$ were formed in the self-assembly process.

Given the aforementioned observations, the self-assembly of triangular fragments were significantly influenced by the position of the extra tpy units. To exclude the possibility of forming prevailing conformations, the theoretical AM1 semi-empirical method was applied to evaluate the rotational barriers around the pivotal arene and the triple bond (black benzene rings labeled with e and g in Scheme 1) for ligands L^4 and L^5 , respectively (Figures S66 and S67). The theoretical calculations showed that in both cases the rotational barriers around the triple bond are low (<2.2 kcal/mol), and the side groups should be freely rotatable at the room temperature. Our previous study indicated that the substituted tpy ligand has a higher binding affinity to Cd^{II} ions.^{12c} Hence, in the presence of an insufficient amount of Cd^{II} ions, the formation of heteroleptic connections should dominate over that of homoleptic ones. Based on this assumption, the stoichiometry-controlled experiment was designed for the mechanistic study. Instead of using 4 equiv of Cd^{II} ions, 2 equiv was applied to trapping the intermediate species. An equimolar mixture of L^1 and L^4 was reacted with 2 equiv of $Cd(NO_3)_2$. The ESI-MS spectrum showed two peaks generated from the 3+ and 4+ ions of $[Cd_2L^1L^4]$ (Figure S59a), implying that two heteroleptic connections between L^1 and L^4 were formed. Because of the geometrical complementarity, the blue-labeled tpy moieties of L^4 were supposedly pinched by L^1 to afford the tetratopic species $[Cd_2L^1L^4]$ (Scheme 3a) where the internal rotation of the outer coordination sites of L^4 relative to the central scaffold was hampered by the dinuclear ring. The

Scheme 3. (a) Proposed Self-Assembly Pathway for $[\text{Cd}_{12}\text{L}^1_3\text{L}^4_3]$ and (b) Possible Structure of $[\text{Cd}_2\text{L}^1\text{L}^5]$



restricted conformation would facilitate the following cooperative coordination to form complex $[\text{Cd}_{12}\text{L}^1_3\text{L}^4_3]$ because the entropy loss from the frozen rotation has been satisfied by the intermolecular heteroleptic complexation. The UV–vis titration was conducted to further corroborate the proposed two-step mechanism. Indeed, an isosbestic point at 326 nm was observed with increasing amount of Cd^{II} up to 2 equiv, indicating the equilibrium between the uncomplexed ligand mixture and intermediate $[\text{Cd}_2\text{L}^1\text{L}^4]$ (Figure S60a). The isosbestic point was slightly shifted to 321 nm by further addition of Cd^{II} to the stoichiometric point, suggesting that a new equilibrium between intermediate $[\text{Cd}_2\text{L}^1\text{L}^4]$ and triangle $[\text{Cd}_{12}\text{L}^1_3\text{L}^4_3]$ was established (Figure S60b).

To reflect how the restricted conformation of $[\text{Cd}_2\text{L}^1\text{L}^4]$ influences the stability of the trimeric hexagonal core held by six homoleptic Cd^{II} connections, complexes $[\text{Cd}_6\text{L}^2_3]$ and $[\text{Cd}_{12}\text{L}^1_3\text{L}^3_3]$ in CD_3CN (1.2×10^{-4} M) were titrated with $\text{Cd}(\text{OTf})_2$ (Figures S68–S70). The ^1H NMR analyses indicated that $[\text{Cd}_6\text{L}^2_3]$ was completely dissociated into $[\text{Cd}_4\text{L}^2]$ when 12 equiv of $\text{Cd}(\text{OTf})_2$ with respect to each homoleptic Cd^{II} center was added. By contrast, 32 equiv of $\text{Cd}(\text{OTf})_2$ was needed to fully break up $[\text{Cd}_{12}\text{L}^1_3\text{L}^4_3]$ into $[\text{Cd}_6\text{L}^1\text{L}^4]$. Because $[\text{Cd}_{12}\text{L}^1_3\text{L}^4_3]$ and $[\text{Cd}_6\text{L}^2_3]$ have the same core structure, the enhanced stability of $[\text{Cd}_{12}\text{L}^1_3\text{L}^4_3]$ could be attributed to its L^1 -regulated conformation. The self-assembly of $[\text{Cd}_{12}\text{L}^1_3\text{L}^4_3]$ might be involved in chelate and/or interannular cooperativity,²² but a more detailed investigation of each isolated binding event is required to quantitatively identify the real occurrence.

On the other hand, when a 1:1 mixture of L^1 and L^5 was treated with 2 equiv of $\text{Cd}(\text{NO}_3)_2$, the ESI-MS study showed the formation of $[\text{Cd}_2\text{L}^1\text{L}^5]$ (Figure S59b). However, in comparison with $[\text{Cd}_2\text{L}^1\text{L}^4]$, no matter where the heteroleptic complexation occurred, the intermediate $[\text{Cd}_2\text{L}^1\text{L}^5]$ would hinder the self-assembly of target triangle $[\text{Cd}_{12}\text{L}^1_3\text{L}^5_3]$ upon treatment with additional Cd^{II} ions. The possible structure of $[\text{Cd}_2\text{L}^1\text{L}^5]$ is illustrated in Scheme 3b, where the orange and purple tpy units of L^5 were complexed with L^1 to generate a distorted dinuclear macrocycle. Accordingly, the model compound L^6 was synthesized to verify whether the heteroleptic complexation with L^1 could take place to produce the geometrically mismatched macrocycle (Figure 4 and Scheme S5). Notably, the complexation reaction of L^1 and

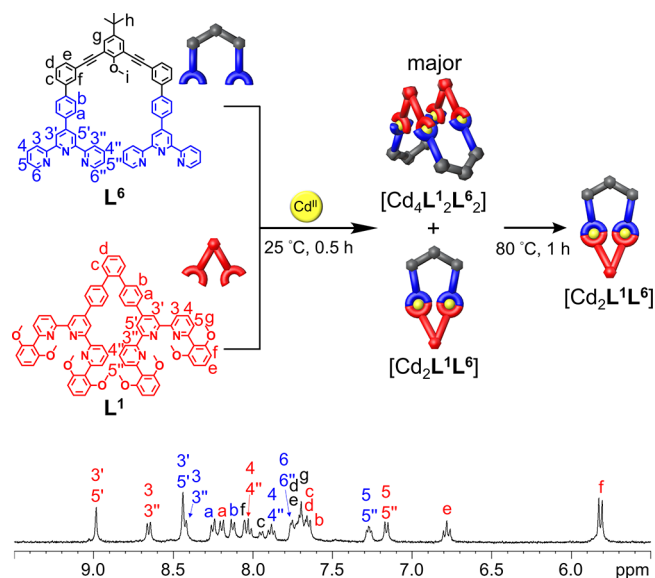


Figure 4. Self-assembly and ^1H NMR spectrum of the distorted dinuclear macrocycle, $[\text{Cd}_2\text{L}^1\text{L}^6]$.

L^6 with Cd^{II} at 25 °C afforded a mixture of $[\text{Cd}_2\text{L}^1\text{L}^6]$ (minor) and $[\text{Cd}_4\text{L}^1_2\text{L}^6_2]$ (major) (Figure S48). After 1 h of heating at 80 °C, the mixture was completely converted into $[\text{Cd}_2\text{L}^1\text{L}^6]$ whose structure was established by NMR and ESI-MS (Figure 4 and Figures S48–S50).

To gain insights into the kinetic aspect, the ligand exchange reaction between a mononuclear heteroleptic complex ($[\text{CdL}^A\text{L}^B](\text{PF}_6)_2$) and a free 6,6''-di(2,6-dimethoxyphenyl)-tpy ligand (L^A) was investigated by ^1H exchange spectroscopy (EXSY) NMR experiments (Figure S71). The exchange rate (k_{ex}) was estimated to be $1.6 \times 10^{-2} \text{ s}^{-1}$ at 25 °C in $\text{CD}_3\text{CN}/\text{CDCl}_3$ (1/1, v/v), which is similar to that ($1.9 \times 10^{-2} \text{ s}^{-1}$) between $[\text{Pd}(\text{py})_4]^{2+}$ (py = pyridine) and free pyridine in CD_3CN .²³ Even though the exchange rate for monotopic ligands is fast, the misassembled yet stable intermediates deduced from multivalent ligand L^5 and ditopic ligand L^1 still interrupted the self-assembly of $[\text{Cd}_{12}\text{L}^1_3\text{L}^5_3]$.

CONCLUSIONS

In summary, a family of multivalent tpy-based ligands L^2 – L^5 were successfully synthesized through Pd-catalyzed cross-couplings and utilized to study the complementary interplay with L^1 . The self-assembly of trimeric hexagon $[\text{Cd}_6\text{L}^2_3]$ was achieved under mild conditions and served as a basis for the following molecular stellation. The star hexagon $[\text{Cd}_{18}\text{L}^1_6\text{L}^3_3]$ was constructed via multicomponent self-assembly, and its structure was established by NMR, ESI-MS, and ESI-TWIM-MS. To understand the assembly mechanism, the self-assembly behavior of two triangular fragments derived from $[\text{Cd}_{18}\text{L}^1_6\text{L}^3_3]$ was investigated by trapping possible intermediates and titration experiments. The mechanistic study manifested that the intermolecular heteroleptic complexation of L^4 or L^5 with L^1 plays a pivotal role in construction of the corresponding triangles. The conformational regulation of L^4 by L^1 could facilitate the formation of the desired triangle $[\text{Cd}_{12}\text{L}^1_3\text{L}^4_3]$ whose assembly process exhibited cooperative coordination. On the other hand, the geometrically mismatched intermediates impeded the self-assembly pathway leading to $[\text{Cd}_{12}\text{L}^1_3\text{L}^5_3]$. We anticipate that this study would

lay the foundation for rationally manipulating metal-mediated cooperative interactions.

■ ASSOCIATED CONTENT

SI Supporting Information

The Supporting Information is available free of charge at <https://pubs.acs.org/doi/10.1021/jacs.0c06618>.

- Experimental details and characterization data (PDF)
Video S1: energy-minimized model of $[\text{Cd}_6\text{L}_3]$ (MOV)
Video S2: energy-minimized model of $[\text{Cd}_{18}\text{L}_6\text{L}_3]$ (MOV)
Video S3: energy-minimized model of $[\text{Cd}_{12}\text{L}_3\text{L}_4]$ (MOV)

■ AUTHOR INFORMATION

Corresponding Author

Yi-Tsu Chan – Department of Chemistry, National Taiwan University, Taipei 10617, Taiwan; orcid.org/0000-0001-9658-2188; Email: ytschan@ntu.edu.tw

Authors

Shi-Cheng Wang – Department of Chemistry, National Taiwan University, Taipei 10617, Taiwan
Kai-Yu Cheng – Department of Chemistry, National Taiwan University, Taipei 10617, Taiwan
Jun-Hao Fu – Department of Chemistry, National Taiwan University, Taipei 10617, Taiwan
Yuan-Chung Cheng – Department of Chemistry, National Taiwan University, Taipei 10617, Taiwan; orcid.org/0000-0003-0125-4267

Complete contact information is available at: <https://pubs.acs.org/doi/10.1021/jacs.0c06618>

Notes

The authors declare no competing financial interest.

■ ACKNOWLEDGMENTS

This research was supported by the Ministry of Science and Technology of Taiwan (MOST106-2628-M-002-007-MY3). We gratefully thank Ms. S.-L. Huang at MOST (National Taiwan University) for the assistance in NMR experiments.

■ REFERENCES

- (1) Whitty, A. Cooperativity and biological complexity. *Nat. Chem. Biol.* **2008**, *4*, 435–439.
- (2) (a) Changeux, J.-P.; Edelstein, S. J. Allosteric Receptors after 30 Years. *Neuron* **1998**, *21*, 959–980. (b) Laos, A. J.; Dean, J. C.; Toa, Z. S. D.; Wilk, K. E.; Scholes, G. D.; Curmi, P. M. G.; Thordarson, P. Cooperative Subunit Refolding of a Light-Harvesting Protein through a Self-Chaperone Mechanism. *Angew. Chem., Int. Ed.* **2017**, *56*, 8384–8388.
- (3) Courey, A. J. Cooperativity in transcriptional control. *Curr. Biol.* **2001**, *11*, R250–R252.
- (4) (a) Takeuchi, M.; Imada, T.; Shinkai, S. A Strong Positive Allosteric Effect in the Molecular Recognition of Dicarboxylic Acids by a Cerium(IV) Bis[tetrakis(4-pyridyl)porphyrinate] Double Decker. *Angew. Chem., Int. Ed.* **1998**, *37*, 2096–2099. (b) Takeuchi, M.; Ikeda, M.; Sugasaki, A.; Shinkai, S. Molecular Design of Artificial Molecular and Ion Recognition Systems with Allosteric Guest Receptors. *Acc. Chem. Res.* **2001**, *34*, 865–873. (c) Tashiro, K.; Aida, T. Metalloporphyrin hosts for supramolecular chemistry of fullerenes. *Chem. Soc. Rev.* **2007**, *36*, 189–197.
- (5) (a) Kovbasyuk, L.; Krämer, R. Allosteric Supramolecular Receptors and Catalysts. *Chem. Rev.* **2004**, *104*, 3161–3188.

- (b) Wiester, M. J.; Ulmann, P. A.; Mirkin, C. A. Enzyme Mimics Based Upon Supramolecular Coordination Chemistry. *Angew. Chem., Int. Ed.* **2011**, *50*, 114–137. (c) Raynal, M.; Ballester, P.; Vidal-Ferran, A.; van Leeuwen, P. W. N. M. Supramolecular catalysis. Part 2: artificial enzyme mimics. *Chem. Soc. Rev.* **2014**, *43*, 1734–1787. (d) Martí-Centelles, V.; Spicer, R. L.; Lusby, P. J. Non-covalent allosteric regulation of capsule catalysis. *Chem. Sci.* **2020**, *11*, 3236–3240. (e) Czescik, J.; Lyu, Y.; Neuberger, S.; Scrimin, P.; Mancin, F. Host–Guest Allosteric Control of an Artificial Phosphatase. *J. Am. Chem. Soc.* **2020**, *142*, 6837–6841.

- (6) (a) Takeuchi, M.; Shioya, T.; Swager, T. M. Allosteric Fluoride Anion Recognition by a Doubly Strapped Porphyrin. *Angew. Chem., Int. Ed.* **2001**, *40*, 3372–3376. (b) Ho, I.-T.; Haung, K.-C.; Chung, W.-S. 1,3-Alternate Calix[4]arene as a Homobinuclear Ditopic Fluorescent Chemosensor for Ag⁺ Ions. *Chem. - Asian J.* **2011**, *6*, 2738–2746. (c) Park, J. S.; Sessler, J. L. Tetrathiafulvalene (TTF)-Annulated Calix[4]pyrroles: Chemically Switchable Systems with Encodable Allosteric Recognition and Logic Gate Functions. *Acc. Chem. Res.* **2018**, *51*, 2400–2410.

- (7) (a) Sprafke, J. K.; Odell, B.; Claridge, T. D. W.; Anderson, H. L. All-or-Nothing Cooperative Self-Assembly of an Annulene Sandwich. *Angew. Chem., Int. Ed.* **2011**, *50*, 5572–5575. (b) Rousseaux, S. A. L.; Gong, J. Q.; Haver, R.; Odell, B.; Claridge, T. D. W.; Herz, L. M.; Anderson, H. L. Self-Assembly of Russian Doll Concentric Porphyrin Nanorings. *J. Am. Chem. Soc.* **2015**, *137*, 12713–12718. (c) Obana, M.; Fukino, T.; Hikima, T.; Aida, T. Self-Sorting in the Formation of Metal–Organic Nanotubes: A Crucial Role of 2D Cooperative Interactions. *J. Am. Chem. Soc.* **2016**, *138*, 9246–9250.

- (8) (a) Harris, K.; Fujita, D.; Fujita, M. Giant hollow MnL₂n spherical complexes: structure, functionalisation and applications. *Chem. Commun.* **2013**, *49*, 6703. (b) Cook, T. R.; Stang, P. J. Recent Developments in the Preparation and Chemistry of Metallacycles and Metallacages via Coordination. *Chem. Rev.* **2015**, *115*, 7001–7045. (c) Chen, L.-J.; Yang, H.-B.; Shionoya, M. Chiral metallosupramolecular architectures. *Chem. Soc. Rev.* **2017**, *46*, 2555–2576. (d) Bloch, W. M.; Clever, G. H. Integrative self-sorting of coordination cages based on ‘naked’ metal ions. *Chem. Commun.* **2017**, *53*, 8506–8516. (e) Chakraborty, S.; Newkome, G. R. Terpyridine-Based Metallosupramolecular Constructs: Tailored Monomers to Precise 2D-Motifs and 3D-Metallocages. *Chem. Soc. Rev.* **2018**, *47*, 3991–4016. (f) Rizzuto, F. J.; von Krbek, L. K. S.; Nitschke, J. R. Strategies for binding multiple guests in metal–organic cages. *Nat. Rev. Chem.* **2019**, *3*, 204–222. (g) Sun, Y.; Chen, C.; Liu, J.; Stang, P. J. Recent developments in the construction and applications of platinum-based metallacycles and metallacages via coordination. *Chem. Soc. Rev.* **2020**, *49*, 3889–3919.

- (9) Hiraoka, S. Unresolved Issues that Remain in Molecular Self-Assembly. *Bull. Chem. Soc. Jpn.* **2018**, *91*, 957–978.

- (10) (a) Yoshizawa, M.; Nagao, M.; Kumazawa, K.; Fujita, M. Side Chain-Directed Complementary Cis-Coordination of Two Pyridines on Pd(II): Selective Multicomponent Assembly of Square-, Rectangular-, and Trigonal Prism-Shaped Molecules. *J. Organomet. Chem.* **2005**, *690*, 5383–5388. (b) Zheng, Y. R.; Zhao, Z.; Wang, M.; Ghosh, K.; Pollock, J. B.; Cook, T. R.; Stang, P. J. A Facile Approach toward Multicomponent Supramolecular Structures: Selective Self-Assembly via Charge Separation. *J. Am. Chem. Soc.* **2010**, *132*, 16873–16882.

- (11) (a) Dietrich-Buchecker, C. O.; Sauvage, J. P.; Kintzinger, J. P. Une nouvelle famille de molecules: les metallo-catenanes. *Tetrahedron Lett.* **1983**, *24*, 5095–5098. (b) Sauvage, J. P.; Weiss, J. Synthesis of biscooper(I) [3]-catenates: multiring interlocked coordinating systems. *J. Am. Chem. Soc.* **1985**, *107*, 6108–6110. (c) Schmittel, M.; Ganz, A. Stable Mixed Phenanthroline Copper(I) Complexes. Key Buildingblocks for Supramolecular Coordination Chemistry. *Chem. Commun.* **1997**, 999–1000. (d) Saha, M. L.; Neogi, S.; Schmittel, M. Dynamic Heteroleptic Metal-Phenanthroline Complexes: from Structure to Function. *Dalton Trans.* **2014**, *43*, 3815–3834.

- (12) (a) Petitjean, A.; Khoury, R. G.; Kyritsakas, N.; Lehn, J.-M. Dynamic Devices. Shape Switching and Substrate Binding in Ion-

Controlled Nanomechanical Molecular Tweezers. *J. Am. Chem. Soc.* **2004**, *126*, 6637–6647. (b) Barboiu, M.; Prodi, L.; Montalti, M.; Zaccheroni, N.; Kyritsakas, N.; Lehn, J. M. Dynamic Chemical Devices: Modulation of Photophysical Properties by Reversible, Ion-Triggered, and Proton-Fuelled Nanomechanical Shape-Flipping Molecular Motions. *Chem. - Eur. J.* **2004**, *10*, 2953–2959. (c) Wang, S.-Y.; Fu, J.-H.; Liang, Y.-P.; He, Y.-J.; Chen, Y.-S.; Chan, Y.-T. Metallo-Supramolecular Self-Assembly of a Multicomponent Ditrigen Based on Complementary Terpyridine Ligand Pairing. *J. Am. Chem. Soc.* **2016**, *138*, 3651–3654. (d) He, Y.-J.; Tu, T.-H.; Su, M.-K.; Yang, C.-W.; Kong, K. V.; Chan, Y.-T. Facile Construction of Metallo-supramolecular Poly(3-hexylthiophene)-*block*-Poly(ethylene oxide) Diblock Copolymers via Complementary Coordination and Their Self-Assembled Nanostructures. *J. Am. Chem. Soc.* **2017**, *139*, 4218–4224. (e) Wang, S.-Y.; Huang, J.-Y.; Liang, Y.-P.; He, Y.-J.; Chen, Y.-S.; Zhan, Y.-Y.; Hiraoka, S.; Liu, Y.-H.; Peng, S.-M.; Chan, Y.-T. Multicomponent Self-Assembly of Metallo-Supramolecular Macrocycles and Cages through Dynamic Heteroleptic Terpyridine Complexation. *Chem. - Eur. J.* **2018**, *24*, 9274–9284.

(13) (a) Ziesel, R. Making New Supermolecules for the Next Century: Multipurpose Reagents from Ethynyl-Grafted Oligopyridines. *Synthesis* **1999**, 1999, 1839–1865. (b) Goodall, W.; Wild, K.; Arm, K. J.; Williams, J. A. G. The synthesis of 4'-aryl substituted terpyridines by Suzuki cross-coupling reactions: substituent effects on ligand fluorescence. *J. Chem. Soc., Perkin Trans. 2* **2002**, 1669–1681. (c) Wang, J.-L.; Li, X.; Lu, X.; Hsieh, I.-F.; Cao, Y.; Moorefield, C. N.; Wesdemiotis, C.; Cheng, S. Z. D.; Newkome, G. R. Stoichiometric Self-Assembly of Shape-Persistent 2D Complexes: A Facile Route to a Symmetric Supramacromolecular Spoked Wheel. *J. Am. Chem. Soc.* **2011**, *133*, 11450–11453.

(14) (a) Zhang, Z.; Li, Y.; Song, B.; Zhang, Y.; Jiang, X.; Wang, M.; Tumbleson, R.; Liu, C.; Wang, P.; Hao, X.-Q.; Rojas, T.; Ngo, A. T.; Sessler, J. L.; Newkome, G. R.; Hla, S. W.; Li, X. Intra- and intermolecular self-assembly of a 20-nm-wide supramolecular hexagonal grid. *Nat. Chem.* **2020**, *12*, 468–474. (b) Wang, G.; Chen, M.; Wang, J.; Jiang, Z.; Liu, D.; Lou, D.; Zhao, H.; Li, K.; Li, S.; Wu, T.; Jiang, Z.; Sun, X.; Wang, P. Reinforced Topological Nanoassemblies: 2D Hexagon-Fused Wheel to 3D Prismatic Metallo-Lamellar Structure with Molecular Weight of 119 K Daltons. *J. Am. Chem. Soc.* **2020**, *142*, 7690–7698.

(15) (a) Jiang, Z.; Li, Y.; Wang, M.; Song, B.; Wang, K.; Sun, M.; Liu, D.; Li, X.; Yuan, J.; Chen, M.; Guo, Y.; Yang, X.; Zhang, T.; Moorefield, C. N.; Newkome, G. R.; Xu, B.; Li, X.; Wang, P. Self-assembly of a supramolecular hexagram and a supramolecular pentagram. *Nat. Commun.* **2017**, *8*, 15476. (b) Song, B.; Kandapal, S.; Gu, J.; Zhang, K.; Reese, A.; Ying, Y.; Wang, L.; Wang, H.; Li, Y.; Wang, M.; Lu, S.; Hao, X.-Q.; Li, X.; Xu, B.; Li, X. Self-assembly of polycyclic supramolecules using linear metal-organic ligands. *Nat. Commun.* **2018**, *9*, 4575. (c) Chen, M.; Wang, J.; Wang, S.-C.; Jiang, Z.; Liu, D.; Liu, Q.; Zhao, H.; Yan, J.; Chan, Y.-T.; Wang, P. Truncated Sierpiński Triangular Assembly from a Molecular Mortise–Tenon Joint. *J. Am. Chem. Soc.* **2018**, *140*, 12168–12174.

(16) Lal Saha, M.; Schmittel, M. Degree of molecular self-sorting in multicomponent systems. *Org. Biomol. Chem.* **2012**, *10*, 4651–4684.

(17) (a) Fu, J. H.; Wang, S. Y.; Chen, Y. S.; Prusty, S.; Chan, Y. T. One-Pot Self-Assembly of Stellated Metallo-supramolecules from Multivalent and Complementary Terpyridine-Based Ligands. *J. Am. Chem. Soc.* **2019**, *141*, 16217–16221. (b) He, L.; Wang, S.-C.; Lin, L.-T.; Cai, J.-Y.; Li, L.; Tu, T.-H.; Chan, Y.-T. Multicomponent Metallo-Supramolecular Nanocapsules Assembled from Calix[4]-resorcinarene-Based Terpyridine Ligands. *J. Am. Chem. Soc.* **2020**, *142*, 7134–7144.

(18) Schubert, U. S.; Winter, A.; Newkome, G. R. In *Terpyridine-Based Materials*; Wiley-VCH Verlag GmbH & Co. KGaA: 2011; pp 65–127.

(19) (a) Giles, K.; Pringle, S. D.; Worthington, K. R.; Little, D.; Wildgoose, J. L.; Bateman, R. H. Applications of a travelling wave-based radio-frequency-only stacked ring ion guide. *Rapid Commun. Mass Spectrom.* **2004**, *18*, 2401–2414. (b) Pringle, S. D.; Giles, K.; Wildgoose, J. L.; Williams, J. P.; Slade, S. E.; Thalassinos, K.; Bateman, R. H.; Bowers, M. T.; Scrivens, J. H. An investigation of the mobility separation of some peptide and protein ions using a new hybrid quadrupole/travelling wave IMS/oa-ToF instrument. *Int. J. Mass Spectrom.* **2007**, *261*, 1–12. (c) Brocker, E. R.; Anderson, S. E.; Northrop, B. H.; Stang, P. J.; Bowers, M. T. Structures of Metallo-supramolecular Coordination Assemblies Can Be Obtained by Ion Mobility Spectrometry-Mass Spectrometry. *J. Am. Chem. Soc.* **2010**, *132*, 13486–13494. (d) Giles, K.; Williams, J. P.; Campuzano, I. Enhancements in travelling wave ion mobility resolution. *Rapid Commun. Mass Spectrom.* **2011**, *25*, 1559–1566. (e) Chan, Y. T.; Li, X.; Yu, J.; Carri, G. A.; Moorefield, C. N.; Newkome, G. R.; Wesdemiotis, C. Design, Synthesis, and Traveling Wave Ion Mobility Mass Spectrometry Characterization of Iron(II)- and Ruthenium(II)-Terpyridine Metallomacrocycles. *J. Am. Chem. Soc.* **2011**, *133*, 11967–11976. (f) Ujma, J.; De Cecco, M.; Chepelin, O.; Levene, H.; Moffat, C.; Pike, S. J.; Lusby, P. J.; Barran, P. E. Shapes of Supramolecular Cages by Ion Mobility Mass Spectrometry. *Chem. Commun.* **2012**, *48*, 4423–4425. (g) Lanucara, F.; Holman, S. W.; Gray, C. J.; Evers, C. E. The Power of Ion Mobility-Mass Spectrometry for Structural Characterization and the Study of Conformational Dynamics. *Nat. Chem.* **2014**, *6*, 281–294. (h) Kalenius, E.; Groessel, M.; Rissanen, K. Ion Mobility–Mass Spectrometry of Supramolecular Complexes and Assemblies. *Nat. Rev. Chem.* **2019**, *3*, 4–14.

(20) Li, X.; Chan, Y.-T.; Newkome, G. R.; Wesdemiotis, C. Gradient Tandem Mass Spectrometry Interfaced with Ion Mobility Separation for the Characterization of Supramolecular Architectures. *Anal. Chem.* **2011**, *83*, 1284–1290.

(21) Wenninger, M. J. *Polyhedron Models*; Cambridge University Press: New York, 1989.

(22) (a) Hunter, C. A.; Anderson, H. L. What is Cooperativity? *Angew. Chem., Int. Ed.* **2009**, *48*, 7488–7499. (b) Ercolani, G.; Schiaffino, L. Allosteric, Chelate, and Interannular Cooperativity: A Mise au Point. *Angew. Chem., Int. Ed.* **2011**, *50*, 1762–1768. (c) von Krbek, L. K. S.; Schalley, C. A.; Thordarson, P. Assessing cooperativity in supramolecular systems. *Chem. Soc. Rev.* **2017**, *46*, 2622–2637.

(23) Sato, S.; Ishido, Y.; Fujita, M. Remarkable Stabilization of M12L24 Spherical Frameworks through the Cooperation of 48 Pd(II)–Pyridine Interactions. *J. Am. Chem. Soc.* **2009**, *131*, 6064–6065.